energies

MDPI

Article

Fabrication and Characterization of $CH_3NH_3PbI_{3-x-y}Br_xCl_y$ Perovskite Solar Cells

Atsushi Suzuki *, Hiroshi Okada and Takeo Oku

Department of Materials Science, the University of Shiga Prefecture, 2500 Hassaka, Hikone, Shiga 522-8533, Japan; me1-bbb4@softbank.ne.jp (H.O.); oku@mat.usp.ac.jp (T.O.)

* Correspondence: suzuki@mat.usp.ac.jp; Tel.: +81-749-28-8369

Academic Editor: Narottam Das

Received: 22 March 2016; Accepted: 6 May 2016; Published: 17 May 2016

Abstract: Fabrication and characterization of $CH_3NH_3PbI_{3-x-y}Br_xCl_y$ perovskite solar cells using mesoporous TiO_2 as electron transporting layer and 2,2′,7,7′-tetrakis-(*N*,*N*-di-4-methoxypheny lamino)-9,9′-spirobifluorene as a hole-transporting layer (HTL) were performed. The purpose of the present study is to investigate role of halogen doping using iodine (I), bromine (Br) and chlorine (Cl) compounds as dopant on the photovoltaic performance and microstructures of $CH_3NH_3PbI_{3-x-y}Br_xCl_y$ perovskite solar cells. The X-ray diffraction identified a slight decrease of crystal spacing in the perovskite crystal structure doped with a small amount of I, Br, and Cl in the perovskite compounds. Scanning electron microscopy (SEM) and energy dispersive X-ray spectroscopy (EDX) showed the perovskite crystal behavior depended on molar ratio of halogen of Pb, I, Br and Cl. Incorporation of the halogen doping into the perovskite crystal structure improved photo generation, carrier diffusion without carrier recombination in the perovskite layer and optimization of electronic structure related with the photovoltaic parameters of open-circuit voltage, short-circuit current density and conversion efficiency. The energy diagram and photovoltaic mechanisms of the perovskite solar cells were discussed in the context of the experimental results.

Keywords: photovoltaic property; perovskite; solar cell; crystal structure; microstructure

1. Introduction

Photovoltaic properties and carrier transport of perovskite based solar cells have been studied for improving charge separation of electrons and holes in a light absorbing layer and carrier transport [1–7]. Organic-inorganic hybrid heterojunction solar cells containing the $CH_3NH_3PbI_3$ perovskite compound have the great advantage of fabricating on mesoporous TiO_2 as the electronic transporting layer and 2,2′,7,7′-tetrakis-(*N*,*N*-di-4-methoxyphenylamino)-9,9′-spirobifluorene (spiro-OMeTAD) as the hole-transporting layer (HTL) [8–10]. The effects of halogen doping and HTL on photovoltaic properties and microstructure on organic-inorganic hybrid heterojunction solar cells using the perovskite compound have been studied for improving photovoltaic performance and optical properties. In particular, the influence of halogen doping on iodide, bromine and chlorine halide perovskite structures in the hybrid solar cells have been characterized for optimizing band gap, crystal structure, optical and photovoltaic properties and conversion efficiency [11–13]. The role of halogen doping using iodine (I), bromine (Br) and chlorine (Cl) compounds as the dopant and the HTL on the photovoltaic and structural properties is an important factor to optimize the improvement of carrier-generation, carrier diffusion, transporting properties and photovoltaic performance. Quantitative investigation into the photovoltaic and optical properties of the perovskite structure with molar ratio dependence of I, Cl and Br compounds has been performed [13]. Control of halogen doping with molar ratio between I, Cl and Br in perovskite crystal structure will provide the best condition for the photovoltaic performance, the crystal structure, carrier mobility and electronic

structure with band gaps between the highest occupied molecular orbital (HOMO) and lowest unoccupied molecular orbital (LUMO) and the optical properties with a wide range of absorption. The insertion of both Cl and Br into the perovskite structure promoted the carrier-generation, and expanded carrier diffusion and lifetime, along with reducing the charge recombination in the active layers for improving the photovoltaic performance [14–20]. A detailed description of the photovoltaic properties, structural analysis, and theoretical investigation using X-ray diffraction pattern (XRD), X-ray photoelectron spectroscopy, scanning electronic microscopy (SEM) and density-functional theory calculation of halogen-doped perovskite layer of $CH_3NH_3PbI_{3-x}Cl_x$, $CH_3NH_3PbBr_{3-x}Cl_x$, $CH_3NH_3SnX_3$ (X = Cl, Br, I), $[HC(NH_2)_2]_{0.83}Cs_{0.17}Pb(I_{0.6}Br_{0.4})_3]$, antimony-doped $CH_3NH_3PbI_3$, $CH_3NH_3Pb_{1-x}Ge_xI_3$, $CH_3NH_3Pb_{1-x}Tl_xI_3$ and $CH_3NH_3Pb_{1-x}In_xI_3$ on TiO_2 layers has been reported [18–29].

The purpose of this study is to investigate influence of halogen doping at variable molar ratio of I, Cl, and Br in inorganic-organic hybrid solar cells using $CH_3NH_3PbI_{3-x-y}Br_xCl_y$ perovskite compounds. The influence of a small amount of halogen doping of I, Cl and Br compounds in the perovskite structure on the photovoltaic and optical properties and charge transport behavior will be investigated for improving the electronic transporting behavior and photovoltaic properties. By using XRD, SEM and energy dispersive X-ray spectroscopy (EDX), microstructure and surface morphologies of the perovskite layer will be confirmed for finding a good condition and optimization within the crystal structure, the carrier transporting properties and the photovoltaic performance. The energy diagram and photovoltaic mechanisms will be discussed for optimization with improvement of the photovoltaic performance and optical absorption.

2. Results

The present photovoltaic cells of fluorine-doped tin-oxide (FTO) FTO/TiO_2/$CH_3NH_3PbI_{3-x-y}Br_xCl_y$/HTL/Au varied with molar ratio at x, y = 0, 1, 2, and 3 were shown in a schematic illustration in Figure 1.

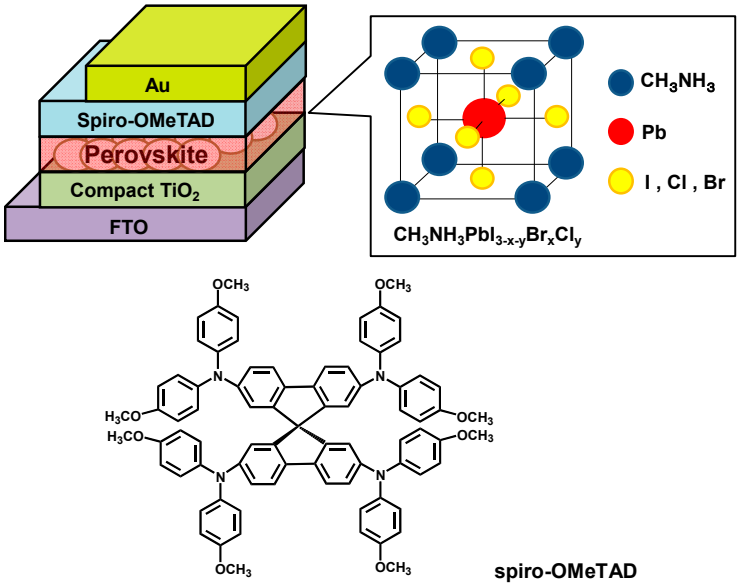

Figure 1. Perovskite solar cell, crystal structure of perovskite and molecular structure of 2,2′,7,7′-tetrakis-(*N*,*N*-di-4-methoxyphenylamino)-9,9′-spirobifluorene (spiro-OMeTAD).

The perovskite solution varied with molar ratio of halogen doping was prepared as listed in Table 1.

Table 1. Recipe of perovskite precursor solution varied with halogen doping at molar ratio.

Halogen Doping	PbI_2	CH_3NH_3I	CH_3NH_3Cl	CH_3NH_3Br
I	1.00	1.00	0.00	0.00
I, Cl	1.00	0.95	0.05	0.00
I, Br	1.00	0.95	0.00	0.05
I, Br, Cl	1.00	0.90	0.05	0.05

The *J-V* characteristics of the perovskite solar cells varied with halogen doping material at certain percentages under illumination are shown in Figure 2.

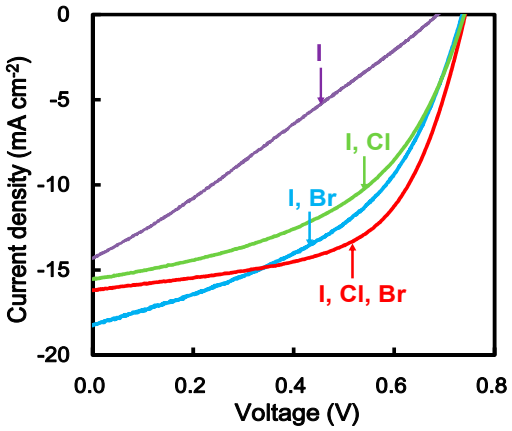

Figure 2. *J-V* Characteristics of fluorine-doped tin-oxide (FTO) FTO/TiO_2/$CH_3NH_3PbI_{3-x-y}Br_xCl_y$/spiro-OMeTAD/Au photovoltaic cells.

The photocurrent was observed under illumination, and the cell structure showed characteristic curves with regard to the short-circuit current density (J_{sc}) and open-circuit voltage (V_{oc}).The detailed parameters of the best device are listed in Table 2. The performance of V_{oc} was increased from 0.69 V to 0.74 V. The short-circuit current density, J_{sc}, was increased from 14.3 mA$\cdot$ cm^{-2} to 16.2 mA$\cdot$ cm^{-2}. Overall power conversion efficiency (*PCE*) was improved from 2.7% to 7.0%. Incorporation of halogen doping of Cl and Br as dopant into the perovskite layer improved the photovoltaic performance of V_{oc}, J_{sc}, fill factor (*FF)* and *PCE* due to optimization of the band gap, extension of carrier diffusion, lifetime, promotion of carrier generation and charge separation with inhibiting carrier recombination in the microstructure. As a standard reference, fabrication and characterization of the reference for halogen doping I in the perovskite structure was repeatedly performed for confirmation of reproducibility. The low conversion seen in producing the sub-reaction of PbI_2 could be caused by degradation with hydrolysis reaction under humidity. Exposure of the perovskite crystal to light and humidity results in the decomposition to PbI_2. While the film preparation and measurements of the *J-V* curve for halogen doping I, Cl and Br in the perovskite solar cells was performed under atmosphere conditions, the photovoltaic parameters of J_{sc}, V_{oc}, *FF* and *PCE* were influenced by the film preparation conditions at normal humidity, such as 40%–60%. The effect of atmospheric humidity on the photovoltaic performance, carrier generation, charge separation and crystallization in the perovskite films has been investigated [30]. The performance of V_{oc} and *FF* with a low efficiency of conversion for halogen doping I in the perovskite solar cell derives from degradation of the crystal growth with carrier loss and leak current near the interface between the crystal domains in microstructure. Optimization of the perovskite crystal growth under the film preparation in a globe box filled with a high purity inert gas will improve the photovoltaic performance of J_{sc}, V_{oc}, *FF*, *PCE* and incident photon to current conversion efficiency (IPCE).

Table 2. Measured parameters of $CH_3NH_3PbI_{3-x-y}Br_xCl_y$ solar cells. *FF*: fill factor; PCE: power conversion efficiency.

Halogen Doping	J_{sc} (mA cm^{-2})	V_{oc} (V)	*FF*	*PCE* (%)
I	14.3	0.686	0.270	2.65
I, Cl	18.2	0.733	0.462	6.17
I, Br	15.5	0.738	0.486	5.56
I, Cl, Br	16.2	0.742	0.582	7.00

Transmission spectra and Tauc-plot of the perovskite solar cells varied with halogen doping of I, Cl and Br as dopants are shown in Figure 3. In the standard condition using halogen doping of I, the absorption of the solar cell was covered in the range of 300–830 nm. Incorporation of halogen doping using Cl and Br as dopants provided a slight drop of absorbance and blue-shift in a wide range of 300–800 nm. While a mixed halogen doping of I, Cl, and Br was added in the perovskite structure, the transmission absorbance decreased with decreasing concentration of I in the perovskite structure. Addition of Cl and Br in the perovskite structure improved the performance of the short-circuit current density, V_{oc}, *FF* and *PCE* for the devices. Introduction of halogen doping with Cl and Br in the perovskite structure optimized the carrier concentration in the perovskite structure, which improved the range of wavelength, the band gap, photo generation and carrier transporting properties and controlled the leakage current.

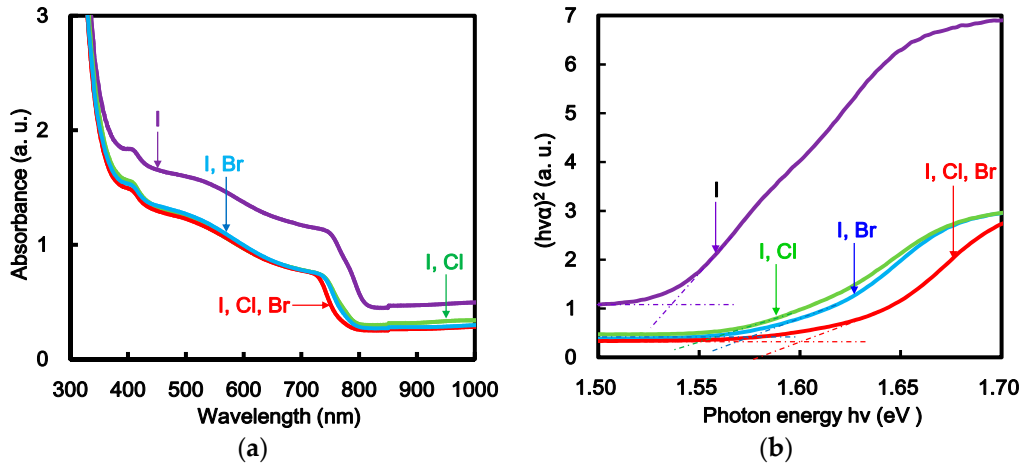

Figure 3. (**a**) Transmission spectra; and (**b**) Tauc-plots of FTO/TiO_2/$CH_3NH_3PbI_{3-x-y}Br_xCl_y$ cells.

The optical energy gap as direct transition was estimated by Tauc-plot. As listed in Table 3, the optical energy gap corresponding to wavelength was obtained to be 1.53 eV and 810 nm in the standard case using halogen doping of I. The optical energy gap was obtained to about 1.60 eV by addition of the halogen doping of I, Cl and Br. Incorporation with a small amount of halogen doping using I, Cl and Br increased the energy gap and carrier transporting behavior. The halogen doping of Cl and Br remarkably influenced the energy gap, wavelength and the photovoltaic performance of J_{sc}, V_{oc} and *PCE*. The role of chloride as dopant on the transporting behavior and the photovoltaic properties on perovskite hybrid solar cells has been discussed [2]. Introducing halogen doping into the perovskite structure controlled the energy gap in the range of wavelengths, which provided the promotion of the photo generation and the carrier transporting properties in the active layer.

The IPCE of the perovskite solar cells with a small amount of halogen doping using I, Cl and Br compounds are shown in Figure 4. In the standard case using halogen doping of I, the performance of IPCE in the solar cells was obtained to be 12%–18% in the range of 400–750 nm. When a mixture of two halogen doping of I and Br was used, IPCE slightly increased to be about 26% at 480 nm. In the case

of two halogen doping with I and Cl, IPCE was increased to be 28%–32% in the range of 550–750 nm. When a mixture of I, Cl and Br was used as a three component system, IPCE slightly decreased to be about 25% at 480 nm. Introduction of halogen doping with I and Cl as dopants optimized the carrier concentration in the perovskite crystal structure for improving band gap, photo generation and carrier transporting properties and controlled the leakage current.

Table 3. Optical band gaps of FTO/TiO_2/$CH_3NH_3PbI_{3-x-y}Br_xCl_y$.

Hydrogen Doping	Wavelength (nm)	Band Gap (eV)
I	810	1.53
I, Cl	800	1.55
I, Br	790	1.57
I, Cl, Br	774	1.60

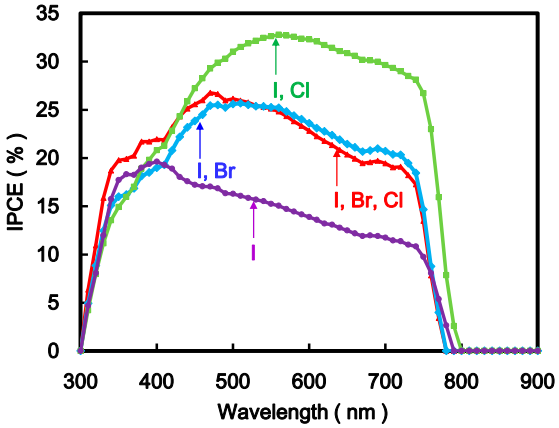

Figure 4. Incident photon to current conversion efficiencies (IPCEs) of FTO/TiO_2/$CH_3NH_3PbI_{3-x-y}Br_xCl_y$/spiro-OMeTAD/Au photovoltaic cells.

Figure 5 shows XRDs of the perovskite solar cells doped with I, Cl and Br. The diffraction patterns of $CH_3NH_3PbI_3$, PbI_2 and TiO_2 were identified as remarks. Under standard conditions of halogen doping of I, a strong diffraction peak in 2θ was obtained to be 14.07°, corresponding to be about 6.29 Å in *d*-spacing. The spacing was assigned to the (100) surface of perovskite crystal structure.

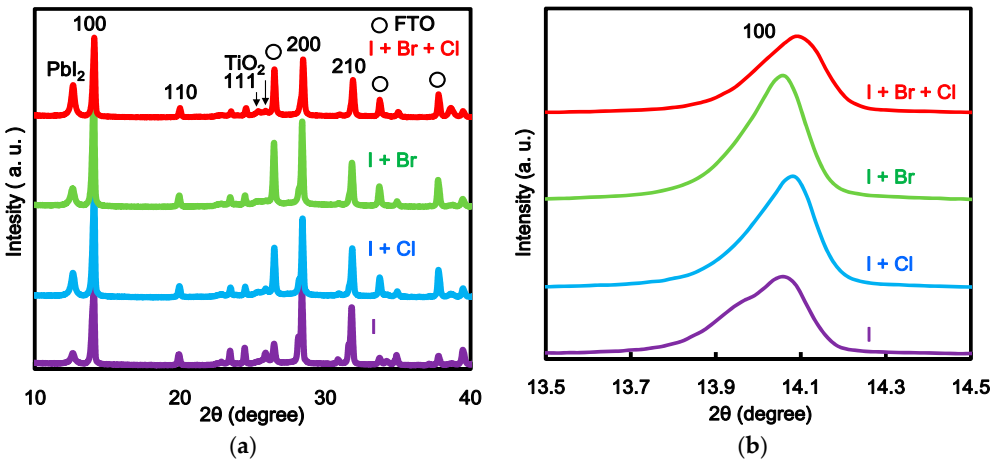

Figure 5. X-ray diffraction patterns (XRDs) of FTO/TiO_2/$CH_3NH_3PbI_{3-x-y}Br_xCl_y$ cells: (**a**) 10° < 2θ < 40°; and (**b**) 13.5° < 2θ < 14.5°.

Table 4 lists the diffraction parameters of 100 of the perovskite crystal structure doped by I, Cl and Br. The lattice constant was slightly decreased by a mixture of halogen doping of I, Cl and Br. The spacing was decreased by addition of Cl and Br compounds as compared with I. The crystallite size increased from 387 Å to 486 Å by addition of the halogen doping using I, Cl and Br. The crystal growth, size and crystal spacing in the perovskite structure was changed by addition of a small amount of halogen doping. Incorporation of I and Cl as dopants into the perovskite crystalline structure dramatically improved the photovoltaic performance, electronic structure, optical absorption, band gap and the transporting behavior within the perovskite layer. Control of chlorine and bromide as dopant is important to optimize the condition of the photo generation, carrier transporting behavior and the photovoltaic performance of J_{sc} and *PCE*.

Table 4. Measured parameters of $CH_3NH_3PbI_{3-x}Br_x$ solar cells.

Halogen Doping	2θ (°)	Lattice Constant (Å)	Crystallite Size (Å)
I	14.07	6.291	387
I, Cl	14.09	6.281	476
I, Br	14.07	6.292	486
I, Cl, Br	14.09	6.282	441

The SEM images of surface morphologies of the perovskite solar cells doped with I, Cl and Br are shown in Figure 6. In the standard case, as shown in Figure 6a, the crystal nucleation in the perovskite layer is caused by the TiO_2 mesoporous surface layer. When a mixture of halogen doping using I, Cl and Br as dopants was added, the perovskite crystal growth gradually accelerated to about 10 μm in diameter on the mesoporous TiO_2 surface layer. From experimental results using XRD and SEM observation, the control of halogen doping condition in the perovskite structure is important to find the best condition for optimization of the crystal growth, the carrier transport properties and the photovoltaic performance.

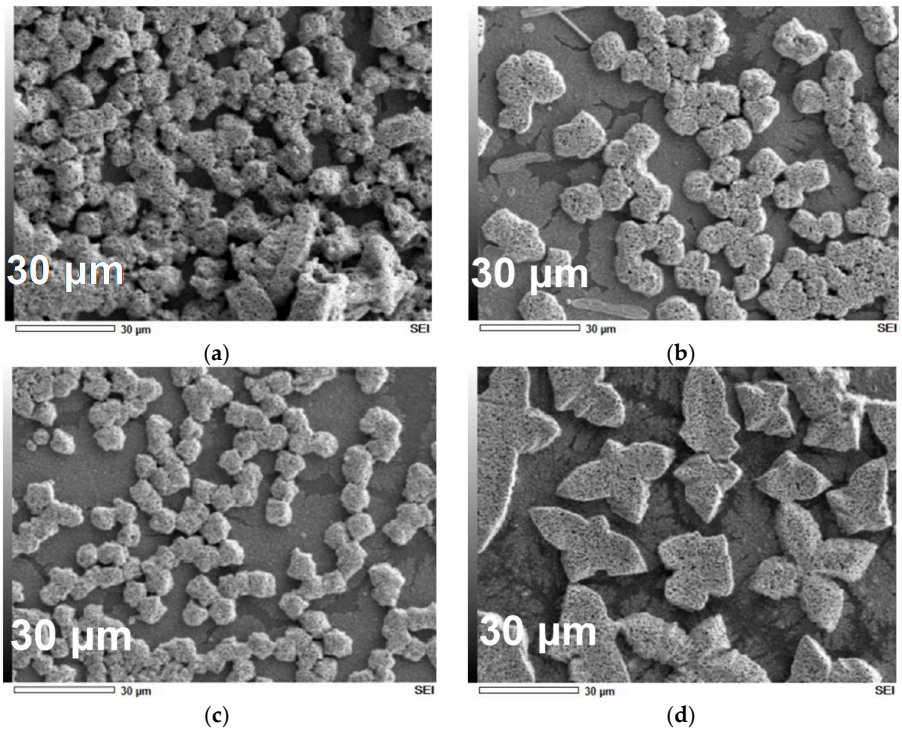

Figure 6. Scanning electron microscopy (SEM) images of FTO/TiO_2/$CH_3NH_3PbI_{3-x-y}Br_xCl_y$ solar cells doped with: (**a**) I; (**b**) I, Cl; (**c**) I, Br; and (**d**) I, Cl, and Br.

Atomic composition on the perovskite layer in the solar cells was analyzed by energy dispersive EDX. The atomic compositions of Pb, I, Cl, and Br in the added case using I, Cl and Br are listed in Table 5. In the standard case using I, the atomic composition of Pb and I was obtained to be 31.0% and 69.0%, yielding molar ratio of 1.0–2.2, which was slightly decreased as compared with halogen doping of Pb and I at molar ratio of 1–3. From the experimental results using the atomic composition of halogen doping using (I, Cl), (I, Br), (I, Cl, Br) as component systems, the molar ratio of Pb to I, Cl and Br was obtained to be 1.00:2.01:0.05:0, 1.00:2.06:0:0.06, and 1.00:1.82:0.05:0.06, respectively. When a mixture of halogen doping of I, Cl, and Br was added as two or three component systems, the halogen doping of Cl and Br diffused in the crystal structure and promoted the crystal growth. This result suggests improvement of the carrier transporting property and the photovoltaic performance of J_{sc} and *PCE* by the halogen doping into the perovskite crystal structure.

Table 5. Atomic composition of halogen atom of the $CH_3NH_3PbI_{3-x-y}Br_xCl_y$ perovskite solar cells.

Halogen Doping	Atomic Composition (%)			
	Pb	I	Cl	Br
I	31.0	69.0	-	-
I, Cl	32.6	65.8	1.62	-
I, Br	32.0	66.0	-	2.03
I, Cl, Br	34.1	62.1	1.72	2.00

3. Discussion

The photovoltaic mechanism of the $CH_3NH_3PbI_{3-x-y}Br_xCl_y$ perovskite solar cells is discussed on the basis of the energy diagram shown in Figure 7. Light irradiation induced the generating and charge separation in $CH_3NH_3PbI_{3-x-y}Br_xCl_y$ as the active layer. The excited electrons of $CH_3NH_3PbI_{3-x-y}Br_xCl_y$ in the conduction band diffused and charges were transferred from $CH_3NH_3PbI_{3-x-y}Br_xCl_y$ to TiO_2 onto the active layer at a FTO substrate. In addition, holes in valence band went through spiro-OMeTAD as HTL and arrived at the Au electrode as the cathode. An energy barrier would exist at the semiconductor–metal interface. The V_{oc} of the perovskite solar cells could be related to the energy gap between the valence band of $CH_3NH_3PbI_{3-x-y}Br_xCl_y$ and conduction band of TiO_2. The energy levels of the HOMO, band gap and the carrier mobility of electron transporting layer could be controlled by combination of hydrogen doping of I, Cl and Br with molar ratio in the perovskite crystal structure [18–27]. Incorporation of Cl and Br as dopants into the perovskite crystalline structure improved the crystal growth and size, the carrier transporting properties and the photovoltaic performance of V_{oc}, J_{sc} and *PCE*. The electron mobility of the perovskite single crystals was 2.5 $cm^2 \cdot V^{-1} \cdot s^{-1}$ [11]. The carrier mobility of the perovskite layer depended on the variable amount of hydrogen doping of I, Cl and Br. It also varied with molar ratio. When the plural halogen doping using I, Cl and Br was used as a two or three component system, the photovoltaic performance, optical properties and band gap were improved as compared with single halogen doping of I.

The control of carrier diffusion, band gap between the energy levels at the conduction and valence bands in the $CH_3NH_3PbI_{3-x-y}Br_xCl_y$ layer is an important factor to improve photovoltaic performance. From the energy diagram and photovoltaic mechanism of the perovskite solar cells, it can be seen that halogen doping of I, Cl and Br in the active layer caused carrier generation, carrier transfer properties and functions, partially because of the electron-transporting layer, improved current density, band gap and conversion efficiency. The photovoltaic performance depends on band gap, carrier mobility and carrier recombination around the interface between the perovskite layer and TiO_2 mesoporous structure as the electron-transporting layer.

In fact, the doping conditions with a small amount of I, Cl and Br in the perovskite layer influenced the crystal spacing and growth of the perovskite structure for improving the carrier diffusion without recombination. The crystalline perovskite structure maintained the photovoltaic and optical properties

by preventing the formation of a leakage current path around the interface. The halogen doping of I, Cl and Br into the perovskite layer have important influences on carrier transporting behavior and the perovskite crystal growth for improving the photovoltaic performance of V_{oc}, J_{sc}, *FF* and *PCE*.

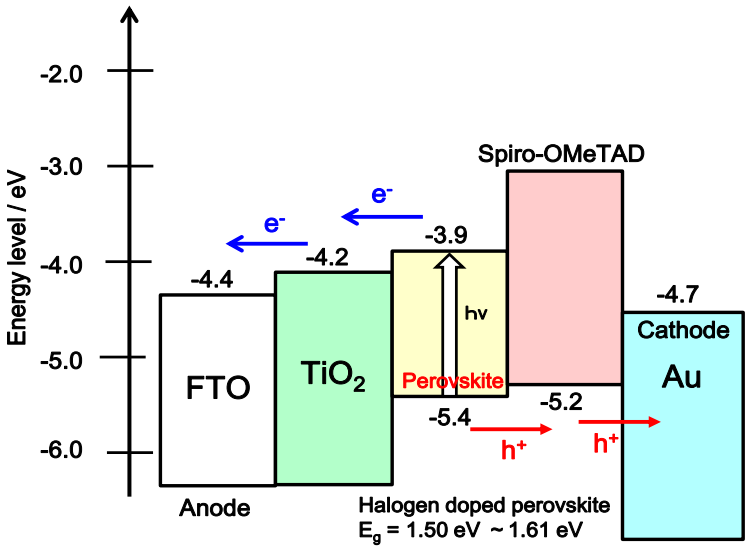

Figure 7. Energy diagram and photovoltaic mechanism of perovskite solar cells.

4. Materials and Methods

FTO-coated glass substrates were cleaned in an ultrasonic bath with acetone and methanol and dried under nitrogen gas. The 0.15 M TiO_2 precursor solution was prepared from titanium diisopropoxide bis(acetylacetonate) (55 µL, Sigma-Aldrich, Tokyo, Japan) in 1-butanol (1 mL), and the TiO_2 precursor solution was spin-coated on the FTO substrate at 3000 rpm for 30 s and annealed 125 °C for 5 min. Afterwards, the coated film was cooled to room temperature, the same process was repeated twice with 0.3 M titanium diisopropoxide bis(acetylacetonate) solution in 1-butanol at 3000 rpm. The coated FTO glasses with TiO_2 precursor solutions were heated at 500 °C for 30 min to form the compact TiO_2 layer. A mesoporous TiO_2 layer was deposited by spin-coating at 5000 rpm for 30 s. TiO_2 paste was prepared with TiO_2 powder (Aerosil P-25, Nippon Aerosil Co. Ltd., Tokyo, Japan) with poly(ethylene glycol) (PEG # 20000, Nacalai Tesque, Inc., Kyoto, Japan) in ultrapure water. The solution was mixed with acetyl acetone (10.0 µL, Wako Pure Chemical Industries, Osaka, Japan) and Triton X-100 (5 µL, Sigma-Aldrich, Tokyo, Japan) for 30 min. The layers were annealed at 500 °C for 30 min. For the preparation of pigment with a perovskite structure, a solution of methyl ammonium iodide (CH_3NH_3I) (Showa Chemical Co. Ltd., Tokyo, Japan), methyl ammonium chloride: (CH_3NH_3Cl) (Showa Chemical Co. Ltd., Tokyo, Japan), methyl ammonium bromide: (CH_3NH_3Br) (Showa Chemical Co. Ltd., Tokyo, Japan) and PbI_2 in γ-butyrolactone (Nacalai Tesque, Inc. Kyoto, Japan) was mixed at 70 °C as listed in Table 1. The solution was then introduced into the TiO_2 mesoporous structure by spin-coating method and annealed at 100 °C for 15 min. As preparation of HTL, a solution of spiro-OMeTAD (36.1 mg, Wako Pure Chemical Industries, Osaka, Japan) in chlorobenzene (0.5 mL, Wako Pure Chemical Industries, Osaka, Japan) was mixed with a solution of lithium bis(trifluoromethylsulfonyl) imide (Li-TFSI, 260 mg, Tokyo Chemical Industry, Tokyo, Japan) in acetonitrile (0.5 mL, Nacalai Tesque, Inc., Kyoto, Japan) for 12 h. The former solution with 4-tert-butylpyridine (14.4 µL Sigma-Aldrich, Tokyo, Japan) was mixed with the Li-TFSI solution (8.8 µL) for 30 min at 70 °C. The HTL solution was prepared on the perovskite structure layer deposed on TiO_2/FTO layer by spin coating. The gold (Au) top electrode was thermally evaporated through a stainless steel mask with an area of 0.090 cm^2 (0.3 cm × 0.3 cm). Layered structures of the present

photovoltaic cells were denoted as FTO/TiO_2/$CH_3NH_3PbI_{3-x-y}Br_xCl_y$/HTL/Au, as shown in a schematic illustration in Figure 1.

The *J-V* characteristics of the photovoltaic solar cells were measured both in the dark and under the illumination at 100 mW· cm^{-2} (AM 1.5 air mass) using a solar simulator (XES-301S, San-ei Electric Co. Ltd., Osaka, Japan) and potentiostat (HSV-110, Hokuto Denko Corporation, Tokyo, Japan). The masked solar cell was 0.090 cm^2 (0.3 cm × 0.3 cm). The photocurrent was observed under illumination, and the cell structure showed characteristic curves with regard to the short-circuit current density (J_{sc}) and open-circuit voltage (V_{oc}). The experimental parameters of forward scan rate, starting and last voltage were fixed to be 100 mV· s^{-1}, −0.2 V and 1.0 V, respectively. Without holding at constant time of the device under illumination in ambient condition, the once scanning of *J-V* curve measurement was performed in the range of forward voltage from −0.2 V to 1.0 V. The hysteresis measurement of photocurrent density with forward and backward voltage was not performed for investigating the transient phenomena. The photovoltaic characterization depended on the film preparation and measurement conditions [31]. Repeated measurements of *J-V* curve were performed for obtaining an average value. The detailed parameters of the best device are listed in Table 2.

Optical absorption properties were investigated by means of ultraviolet-visible-near-infrared spectroscopy (Jasco V-670, Jasco Corporation, Tokyo, Japan). Optical band gap as direct transition of the perovskite solar cells doped with I, Cl and Br was estimated by Tauc-plot. The X-ray diffraction measurements were performed and equipped with a monochromatic CuKα X-ray source (λ = 0.15418 nm) (Bruker D2 PHASER, Bruker Corporation, Billerica, MA, USA). Surface morphology was observed by optical microscopy (Nikon eclipse E600, Nikon Corporation, Tokyo, Japan) and analytical SEM (JEOL JSM-6010 PLUS/LA, JEOL Ltd., Tokyo, Japan). Atomic composition on the perovskite layer in the solar cells was analyzed by energy dispersive EDX. The external quantum efficiency (EQE) values of the solar cells (Enlitech QE-R3011, Enlitech Technology Co. Ltd., Kaohsiung, Taiwan) were measured. The device active area for all the solar cells was 0.090 cm^2.

5. Conclusions

Fabrication and characterization of $CH_3NH_3PbI_{3-x-y}Br_xCl_y$ perovskite solar cells using mesoporous TiO_2 as the electronic transporting layer and spiro-OMeTAD as the HTL were carried out. The effect of halogen doping using I, Br and Cl compounds as dopant on the photovoltaic, optical properties and crystal structures of the perovskite-based solar cells was investigated. When a mixture of halogen dopants using I, Cl and Br was added into the perovskite structure, the photovoltaic performance of J_{sc}, V_{oc}, *FF*, *PCE*, optical wavelength and crystalline growth behavior were improved in comparison with other cases using single halogen doping with I, Cl and Br. The XRD confirmed a slight decrease of lattice constant of the perovskite structure doped with I, Br, and Cl in the solar cell. SEM and energy dispersive EDX identified the crystalline growth behavior by enhancing the crystal size, and determined molar ratio of Pb, I, Br and Cl in the $CH_3NH_3PbI_{3-x-y}Br_xCl_y$ perovskite structure. Incorporation of the halogen doping using Pb, I, Br and Cl in the crystal structure promoted the photo generation and carrier diffusion with suppressing carrier recombination in the crystal structure, and optimized the electron structure with a slight change of band gap, improving the photovoltaic performance of $V_{oc,}$ J_{sc} and IPCE. The photovoltaic mechanism of the perovskite solar cells was discussed in the context of the experimental results.

Acknowledgments: This work was supported by JSPS KAKENHI Grant No. 26390047.

Author Contributions: Atsushi Suzuki and Hiroshi Okada conceived and designed the experiments; Hiroshi Okada performed the experiments; Hiroshi Okada and Atsushi Suzuki analyzed the data; Atsushi Suzuki and Takeo Oku contributed reagents/materials/analysis tools; Atsushi Suzuki wrote the paper.

Conflicts of Interest: The authors declare no conflict of interest.

References

1. Heo, J.H.; Im, S.H.; Noh, J.H.; Mandal, T.N.; Lim, C.S.; Chang, J.A.; Lee, Y.H.; Kim, H.J.; Sarkar, A.; Nazeeruddin, M.K.; *et al.* Efficient inorganic organic hybrid heterojunction solar cells containing perovskite compound and polymeric hole conductors. *Nat. Photonics* **2013**, *7*, 486–491. [CrossRef]
2. Colella, S.; Mosconi, E.; Fedeli, P.; Listorti, A.; Gazza, F.; Orlandi, F.; Ferro, R.; Besagni, T.; Rizzo, A.; Calestani, G.; *et al.* $MAPbI_{3-x}Cl_x$ mixed halide perovskite for hybrid solar cells: The role of chloride as dopant on the transport and structural properties. *Chem. Mater.* **2013**, *25*, 4613–4618. [CrossRef]
3. Zushi, M.; Suzuki, A.; Akiyama, T.; Oku, T. Fabrication and characterization of $TiO_2/CH_3NH_3PbI_3$-based photovoltaic devices. *Chem. Lett.* **2014**, *43*, 916–918. [CrossRef]
4. Oku, T.; Zushi, M.; Imanishi, Y.; Suzuki, A.; Suzuki, K. Microstructures and photovoltaic properties of perovskite-type $CH_3NH_3PbI_3$ compounds. *Appl. Phys. Express* **2014**, *7*. [CrossRef]
5. Suzuki, A.; Kida, T.; Takagi, T.; Oku, T. Effects of hole-transporting layers of perovskite-based solar cells. *Jpn. J. Appl. Phys.* **2016**, *55*. [CrossRef]
6. Qin, P.; Paek, S.; Dar, M.I.; Pellet, N.; Ko, J.; Grätzel, M.; Nazeeruddin, M.K. Perovskite solar cells with 12.8% efficiency by using conjugated quinolizino acridine based hole transporting material. *J. Am. Chem. Soc.* **2014**, *136*, 8516–8519. [CrossRef] [PubMed]
7. Qin, P.; Tanaka, S.; Ito, S.; Tetreault, N.; Manabe, K.; Nishino, H.; Khaja, M.; Grätzel, M. Inorganic hole conductor-based lead halide perovskite solar cells with 12.4% conversion efficiency. *Nat. Commun.* **2014**, *5*. [CrossRef] [PubMed]
8. Jeon, N.J.; Noh, J.H.; Kim, Y.C.; Yang, W.S.; Ryu, S.; Seok, S.I. Solvent engineering for high-performance inorganic-organic hybrid perovskite solar cells. *Nat. Mater.* **2014**, *13*, 897–903. [CrossRef] [PubMed]
9. Kumar, C.V.; Sfyri, G.; Raptis, D.; Stathatos, E.; Lianos, P. Perovskite solar cell with low cost Cu-phthalocyanine as hole transporting material. *RSC Adv.* **2015**, *5*, 3786–3791. [CrossRef]
10. Sfyri, G.; Kumar, C.V.; Sabapathi, G.; Giribabu, L.; Andrikopoulos, K.S.; Stathatos, E.; Lianos, P. Subphthalocyanine as hole transporting material for perovskite solar cells. *RSC Adv.* **2015**, *5*, 69813–69818. [CrossRef]
11. Ramos, F.J.; Ince, M.; Urbani, M.; Abate, A.; Grätzel, M.; Ahmad, S.; Torres, T.; Nazeeruddin, M.K. Non-aggregated Zn(II)octa(2,6-diphenylphenoxy) phthalocyanine as a hole transporting material for efficient perovskite solar cells. *Dalton Trans.* **2015**, *44*, 10847–10851. [CrossRef] [PubMed]
12. Shi, D.; Adinolti, V.; Comin, R.; Yuan, M.; Alarousu, E.; Buin, A.; Chen, Y.; Hoogland, S.; Rothenberger, A.; Katsiev, K.; *et al.* Low trap-state density and long carrier diffusion in organolead trihalide perovskite single crystals. *Science* **2015**, *30*, 519–522. [CrossRef] [PubMed]
13. Cojocaru, L.; Uchida, S.; Jena, A.K.; Miyasaka, T.; Nakazaki, J.; Kubo, T.; Segawa, H. Determination of chloride content in planar $CH_3NH_3PbI_{3-x}Cl_x$ solar cells by chemical analysis. *Chem. Lett.* **2015**, *44*, 1089–1091. [CrossRef]
14. Edri, E.; Kirmayer, S.; Kulbak, M.; Hodes, G.; Cahen, D. Chloride inclusion and hole transport material doping to improve methyl ammonium lead bromide perovskite-based high open-circuit voltage solar cells. *J. Phys. Chem. Lett.* **2014**, *5*, 429–433. [CrossRef] [PubMed]
15. Chen, Q.; Zhou, H.; Fang, Y.; Stieg, A.Z.; Song, T.B.; Wang, H.-H.; Xu, X.; Liu, Y.; Lu, S.; You, J.; *et al.* The optoelectronic role of chlorine in $CH_3NH_3PbI_3$(Cl)-based perovskite solar cells. *Nat. Commun.* **2015**, *6*. [CrossRef] [PubMed]
16. Xu, Y.; Zhu, L.; Shi, J.; Lv, S.; Xu, X.; Xiao, J.; Dong, J.; Wu, H.; Luo, Y.; Li, D.; *et al.* Efficient hybrid mesoscopic solar cells with morphology-controlled $CH_3NH_3PbI_{3-x}Cl_x$ derived from two-step spin coating method. *ACS Appl. Mater. Interfaces* **2015**, *7*, 2242–2248. [CrossRef] [PubMed]
17. Qing, J.; Chandran, H.-T.; Cheng, Y.-H.; Liu, X.-K.; Li, H.-W.; Tsang, S.-W.; Lo, M.-F.; Lee, C.-S. Chlorine incorporation for enhanced performance of planar perovskite solar cell based on lead acetate precursor. *ACS Appl. Mater. Interfaces* **2015**, *7*, 23110–23116. [CrossRef] [PubMed]
18. Dimesso, L.; Dimamay, M.; Hamburger, M.; Jaegermann, W. Properties of $CH_3NH_3PbX_3$ (X = I, Br, Cl) powders as precursors for organic/inorganic solar cells. *Chem. Mater.* **2014**, *26*, 6762–6770. [CrossRef]
19. Dharani, S.; Dewi, H.A.; Prabhakar, R.R.; Baikie, T.; Shi, C.; Yonghua, D.; Mathews, N.; Boix, P.P.; Mhaisalkar, S.G. Incorporation of Cl into sequentially deposited lead halide perovskite films for highly efficient mesoporous solar cells. *Nanoscale* **2014**, *6*, 13854–13860. [CrossRef] [PubMed]

20. Shi, T.; Yin, W.-J.; Hong, F.; Zhu, K.; Yan, Y. Unipolar self-doping behavior in perovskite $CH_3NH_3PbBr_3$. *Appl. Phys. Lett.* **2015**, *106*. [CrossRef]
21. Feng, J.; Xiao, B. Effective masses and electronic and optical properties of nontoxic $MASnX_3$ (X = Cl, Br, and I) perovskite structures as solar cell absorber: A theoretical study using HSE06. *J. Phys. Chem. C* **2014**, *118*, 19655–19660. [CrossRef]
22. McMeekin, D.P.; Sadoughi, G.; Rehman, W.; Eperon, G.E.; Saliba, M.; Hörantner, M.T.; Haghighirad, A.; Sakai, N.; Korte, L.; Rech, B.; *et al.* A mixed-cation lead mixed-halide perovskite absorber for tandem solar cells. *Science* **2016**, *351*, 151–155. [CrossRef] [PubMed]
23. Yi, C.; Luo, J.; Meloni, S.; Boziki, A.; Astani, N.A.; Grätzel, C.; Zakeeruddin, S.M.; Röthlisberger, U.; Grätzel, M. Entropic stabilization of mixed A-cation ABX_3 metal halide perovskites for high performance perovskite solar cells. *Energy Environ. Sci.* **2016**, *9*, 656–662. [CrossRef]
24. Suzuki, K.; Suzuki, A.; Zushi, M.; Oku, T. Microstructures and Properties of $CH_3NH_3PbI_{3-x}Cl_x$ Hybrid Solar Cells. In Proceedings of the AIP Conference, Ibaraki, Japan, 6–7 November 2014; pp. 96–101.
25. Suzuki, A.; Okada, H.; Oku, T. Role of Bromine Doping on the Photovoltaic Properties and Microstructures of $CH_3NH_3PbI_3$ Perovskite Solar Cells. In Proceedings of the AIP Conference, Aichi, Japan, 22–23 October 2015.
26. Oku, T.; Ohishi, Y.; Suzuki, A. Effects of antimony addition to perovskite-type $CH_3NH_3PbI_3$ photovoltaic devices. *Chem. Lett.* **2016**, *45*, 134–136. [CrossRef]
27. Saito, J.; Oku, T.; Suzuki, A.; Akiyama, T. Fabrication and Characterization of Perovskite-Type Solar Cells with Nb-Doped TiO_2 Layers. In Proceedings of the AIP Conference, Aichi, Japan, 22–23 October 2015.
28. Ohishi, Y.; Oku, T.; Suzuki, A. Fabrication and Characterization of Perovskite-Based $CH_3NH_3Pb_{1-x}Ge_xI_3$, $CH_3NH_3Pb_{1-x}Tl_xI_3$ and $CH_3NH_3Pb_{1-x}In_xI_3$ Photovoltaic Devices. In Proceedings of the AIP Conference, Aichi, Japan, 22–23 October 2015.
29. Oku, T.; Suzuki, K.; Suzuki, A. Effects of chlorine addition to perovskite-type $CH_3NH_3PbI_3$ photovoltaic devices. *J. Ceram. Soc. Jpn.* **2016**, *124*, 234–238. [CrossRef]
30. Christians, J.A.; Manser, J.S.; Kamat, P.V. Multifaceted excited state of $CH_3NH_3PbI_3$. Charge separation, recombination, and trapping. *Phys. Chem. Lett.* **2015**, *6*, 2086–2095. [CrossRef] [PubMed]
31. Christians, J.A.; Manser, J.S.; Kamat, P.V. Best practices in perovskite solar cell efficiency measurements. Avoiding the error of making bad cells look good. *J. Phys. Chem. Lett.* **2015**, *6*, 852–857. [CrossRef] [PubMed]